

Full Length Article

3D spatial distribution of *Sost* mRNA and sclerostin protein expression in response to in vivo tibia loading in female mice

Quentin A. Meslier^{a,c,*}, Jacy Hoffmann^a, Robert Oehrlein^a, Daniel Kurczy^a, James R. Monaghan^{a,b,d}, Sandra J. Shefelbine^{a,d}

^a Department of Bioengineering, Northeastern University, Boston, MA, United States

^b Department of Biology, Northeastern University, Boston, MA, United States

^c LifeCanvas Technologies, Cambridge, MA, United States

^d Institute for Chemical Imaging of Living Systems, Northeastern University, Boston, MA, United States

ARTICLE INFO

Keywords:

Bone
Osteocytes
Mechanoadaptation
Sclerostin
Tissue clearing
3D immunolabeling
3D fluorescence in situ hybridization

ABSTRACT

Bones adapt to external mechanical loads through a process known as mechanoadaptation. Osteocytes are the bone cells that sense the mechanical environment and initiate a biological response. Investigating the changes in osteocyte molecular expression following mechanical loading has been instrumental in characterizing the regulatory pathways involved in bone adaptation. However, current methods for examining osteocyte molecular expression do not preserve the three-dimensional structure of the bone, which plays a critical role in the mechanical stimuli sensed by the osteocytes and their spatially controlled biological responses.

In this study, we used WISH-BONE (Whole-mount In Situ Histology of Bone) to investigate the spatial distribution of *Sost*-mRNA transcripts and its encoded protein, sclerostin, in 3D mouse tibia midshaft following in vivo tibia loading. Our findings showed a decrease in the percentage of *Sost*-positive osteocytes, after loading, along the posterior-lateral side of the tibia. The number of sclerostin-positive osteocytes were found to significantly decrease at a very specific 2D location of the tibia after loading. However, in 3D, the total number of sclerostin-positive osteocytes was similar between loaded and control legs.

This work is the first to provide a 3D analysis of *Sost* and sclerostin distribution in loaded versus contralateral mouse tibia midshafts. It also highlights the importance of the bone region analyzed and the method utilized when interpreting mechanoadaptation results. WISH-BONE represents a powerful tool for further characterization of mechanosensitive genes regulation in bone and holds the potential for advancing the development of new treatments targeting mechanosensitivity-related bone disorders.

1. Introduction

Osteocytes are the managers of the adaptation response in bone. They are responsible for sensing the external mechanical stimuli applied to the bone and initiating a biological response, resulting in changes to bone homeostasis. Stimulation of the osteocytes *in vivo* can be achieved using uniaxial compression models which have been used to stimulate mouse tibiae [1,2] or rat and mouse ulnae [3] and investigate bone mechanoadaptation response. Mechanical stimuli, when above a certain threshold, have been reported to induce an increase in bone mass and bone formation rate for example. Loading parameters have been shown to play a critical role in the bone response such as loading magnitude, frequency, rate, loading duration, and more [4,5]. Under compression,

the bone anabolic response has been predominantly observed in regions where the mechanical stimulus is known to be high, such as the posterior-lateral side of the tibia for example [6,7]. These responses at the tissue level are in part due to a change in the osteocyte's molecular activity.

Investigations of osteocytes' molecular expression in response to loading have provided a greater understanding of the molecular pathways involved in mechanoadaptation. However, current methods to analyze gene expression in bone cells require homogenization (RNA-Seq and rt-PCR), or sectioning of the bone (In Situ Hybridization), losing 3D spatial information. Under compression, bones mechanical environment varies along the bone length. For example, the posterior side of the mouse tibia is in compression whereas the anterior side is in tension

* Corresponding author at: Department of Bioengineering, Northeastern University, Boston, MA, United States.

E-mail address: meslier.q@northeastern.edu (Q.A. Meslier).

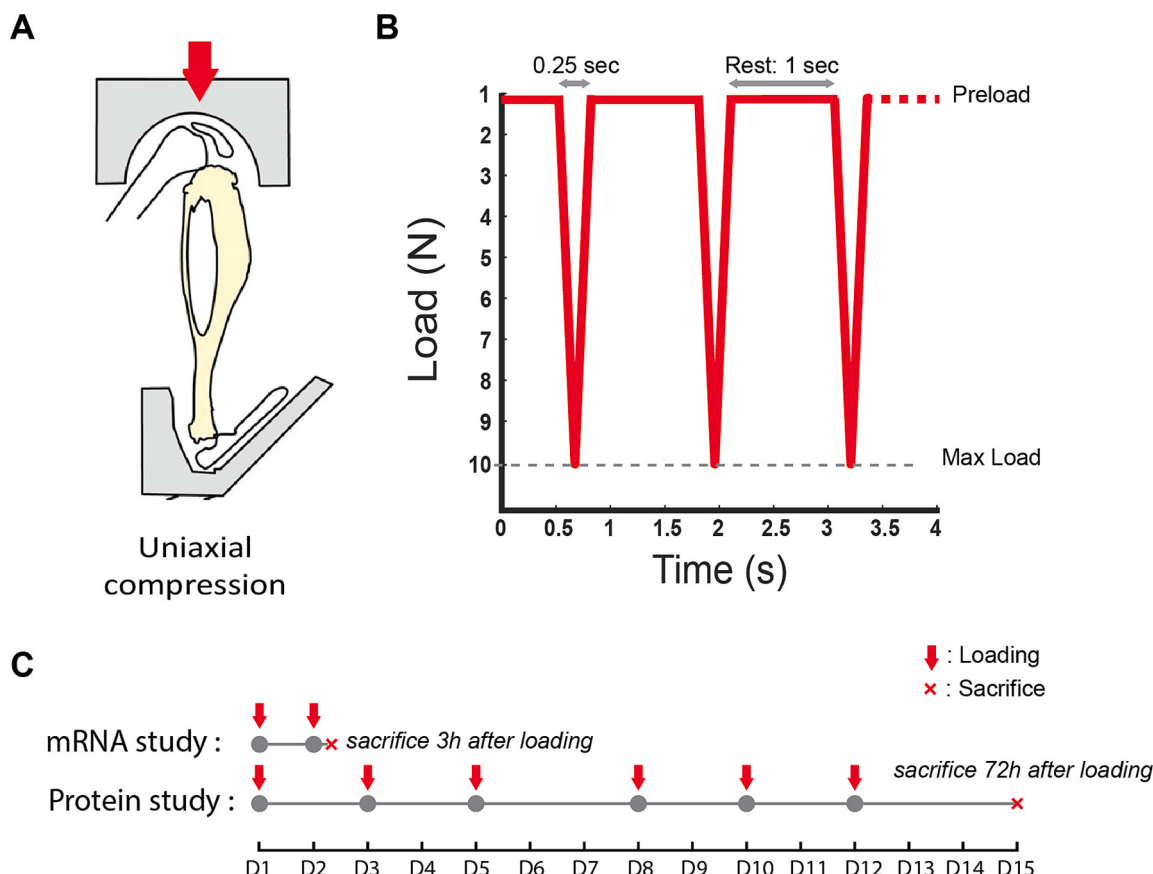


Fig. 1. *In vivo* loading experiment summary. A) Illustration of the *in vivo* uniaxial tibia compression model. The red arrow corresponds to the direction of the compression. B) Loading profile applied on the mouse tibia. A 10 N triangle loading profile was applied *in vivo* to the mouse tibia using with a 1 N preload, 0.25 sec loading time, and 1 sec rest period between cycles. Loading cycles were applied 100 times. C) Experimental timeline. For mRNA analysis, loading was performed 24 h and 3 h before samples collection. For protein labeling, the mice's right tibia was loaded 3 days a week for 2 weeks. Mice were then sacrificed 72 h after the last loading session. (For interpretation of the references to color in this figure legend, the reader is referred to the web version of this article.)

during tibial compression [7–9]. Moreover, the magnitude of mechanical stimuli (strain, fluid flow, and others) spatially varies in the bone which may locally regulate the biological response. Spatial heterogeneity is challenging to capture using tissue sections or methods extracting the molecules of interest out of the samples as they fail to maintain the 3D structure of the bone.

Sclerostin has been shown to play a critical role in bone mechanoadaptation. Sclerostin is released by the osteocytes and prevents bone formation by inhibiting the Wnt/β-catenin pathway. Studies have reported downregulation of sclerostin expression in the osteocytes 24 h after 2 consecutive days of bone mechanical stimulation [7,10,11]. An increase in bone formation has been correlated with strain magnitudes and down-regulation of sclerostin expression. In cross-sections, the decrease in osteocytes expressing sclerostin was greater in regions experiencing high strain magnitude [7,12]. Further studies demonstrated downregulation of *Sost*, between 3 h and 24 h after loading, in mouse tibia using RT-PCR [13], RNA sequencing data, and *in situ* hybridization [14,15]. In hindlimb unloading models, which reduce the mechanical stimulation in the bone, *Sost* mRNA expression increased, but there was no change in sclerostin protein expression in mouse tibiae [12].

However, mRNA and protein analyses are commonly performed in a whole homogenized portion of the bone or a few thin 2D sections at specific locations of the bone length, limiting the number of cells analyzed. It also reflects the biological response at one specific location, which might not be representative of the biological response in the entire bone and might participate in an incomplete interpretation of the results.

The recently developed WISH-BONE methods (Whole-mount In Situ Histology of Bone) allows to separately label abundant genes and protein in 3D in adult mouse bones [16]. The WISH-BONE methods enable the investigation of hundreds of thousands of cells in the entire tibia midshaft providing a more complete interpretation of the impact of mechanical stimuli on the regulation of molecular expression. Until now, investigation of the osteocyte's response to external loads in 3D was limited due to labeling and imaging challenges.

In this work, we used our recently developed methods, WISH-BONE, to investigate the change in osteocytes expressing *Sost* mRNA in 3D, 24 h after uniaxial tibia loading in adult mice. We also investigated the percentage of osteocytes expressing sclerostin after 2 weeks of tibia loading. We hypothesize that regulation of *Sost* expression is dependent on the mechanical environment and therefore spatially varying in 3D with local variations matching known variations in the mechanical environment. We report a decrease of *Sost* mRNA signal in the loaded legs mostly on the posterior-lateral side where the mechanical stimulus is known to be the highest under compression. A decline in protein expression after 2 weeks of loading was captured only at very specific locations. This novel way to explore the regulation of mechanosensitive genes and encoded proteins should provide new insights into bone mechanosensitivity and help inform the design of new treatment strategies for bone mass loss.

2. Methods

2.1. *In vivo* tibia loading

All experiments were approved by Northeastern University's

Institutional Animal Care and Use Committee (IACUC). 22-week-old female C57BL/6 J mice were purchased from Jackson Laboratories. Mice were housed in cages of 5, under normal diet, with a 12-h dark and light cycle, and aged to 23 weeks old. A total of 10 mice were used in this study.

In this study, we used the uniaxial tibia compression model [1,2]. Mice were placed under anesthesia using 2 % isoflurane. The right legs of 23-week-old mice were loaded using the ElectroForce 5500 (TA instruments, USA). A 10 N triangle loading profile was applied over 0.25 s (4 Hz), with a load rate of 72 N/s. A 1 s rest period was inserted between each cycle. A total of 100 cycles were applied per loading bout. Left legs were kept as contralateral control for comparison. This loading profile has been commonly used in the literature and has been shown to induce mechanoadaptation response in tibia midshafts from adult female mice [2,5,6,9,17]. This loading profile has been estimated to induce a strain magnitude of about 2000 microstrains in the anterior-medial tibia (site in tension) [9,18]. This target deformation has been commonly used in the literature to induce bone adaptation in different experimental models [6,10,12,19].

To evaluate how *Sost* mRNA expression varies spatially in 3D ($n = 5$), 2 loading bouts were applied on the right legs, 24 h and 3 h before sacrifice. For the investigation of sclerostin protein expression spatially ($n = 5$), loading was applied 3 days a week for 2 weeks, which is a commonly used protocol for assessing bone adaptation. Mice were sacrificed 3 days after the last loading bouts. The *in vivo* loading experiment is summarized in Fig. 1-A, 1-B, 1-C.

2.2. Sample collection, fixation, and decalcification

23-week-old mice (mRNA labeling) and 25-week-old mice (protein labeling) were sacrificed via CO₂ inhalation and cervical dislocation. Loaded and contralateral tibiae were collected, and external tissues were removed from the bones. The distal end of the tibiae was removed, and the bone marrow was flushed from the proximal end using 1 ml of 1× phosphate buffer saline (PBS). Samples were then immersed in 4 % iced-cold paraformaldehyde (PFA) for 24 h at 4 °C with shaking for fixation. The fixative solution was washed 3 times using 1xPBS and bones were decalcified in 10 % EDTA for 2 weeks at 4 °C with shaking. EDTA was replaced every 3 days. After decalcification, samples were washed in water and stored in PBS at 4 °C.

2.3. 3D mRNA labeling

The mRNA labeling protocol was presented in detail in our previous WISH-BONE method and was adapted from previously described protocols [20,21]. We outline the method briefly here.

Once decalcified, samples were dehydrated using multiple 15 min incubation steps in increasing concentration of methanol (MeOH): 25 %, 50 %, 75 %, 100 %, and 100 % MeOH prepared in 1xPBS with 1 % Tween (PBST) and stored in -20 °C overnight. Samples were then rehydrated via successive baths of MeOH of decreasing concentration (75 %, 50 %, 25 % MeOH in PBST) followed by two 15 min incubations in 100 % PBST at room temperature (RT). Samples were briefly permeabilized in proteinase k (10 µg/ml) for 15 min at RT, post-fixed with 4 % PFA for 20 min, and washed 3 times in 1xPBS. Samples were washed in hybridization buffer for 5 min and then prehybridized for 30 min at 37 °C. Probe solutions were prepared by diluting the probes at 1:200 in 30 % formamide hybridization buffer to a final concentration of 5 µM. Samples were incubated in probe solution overnight at 37 °C for hybridization. Preheated 30 % formamide wash solution was used to wash out unbound probes by incubating samples 4x15min at 37 °C. Samples were then further washed using 5× saline-sodium citrate with 10 % Tween (5xSSCT). Samples were incubated in an amplification buffer at RT for 30 min. DNA hairpins were preheated at 90 °C for 1 min, 30s to ensure proper DNA folding prior to applying to initiators. Hairpins are then cooled to RT for at least 30 min. The hairpin solution was prepared

in an amplification buffer at a final concentration of 60 nM. Samples were incubated in hairpin solution overnight protected from the light. Finally, samples were washed using 5xSSCT and nuclear staining was performed by incubation of the sample with Oxazole Yellow in 1xPBS (1:1000).

To validate labeling, control samples were incubated only with fluorescent DNA hairpins but no DNA probes, which helped quantify potential signals from non-specific bindings of the fluorescent hairpins in the samples.

2.4. 3D protein labeling

Using the WISH-BONE method [16], decalcified samples were preserved using SHIELD (LifeCanvas Technologies, Cambridge). First, an overnight incubation, at 4 °C, in 5 ml SHIELD OFF solution (50 % SHIELD-epoxy, 25 % SHIELD Buffer, and 25 % water) was performed to let the SHIELD-epoxy diffuse in the samples. Next samples were incubated in SHIELD ON solution combined with 1 % SHIELD-epoxy at 37 °C overnight. The SHIELD ON solution allowed the epoxy to polymerize and preserve the sample while adding 1 % of SHIELD-epoxy ensured the good preservation of the bone surfaces. The following day, samples were washed 3 times in 1xPBS to complete sample preservation. Once preserved samples were permeabilized using collagenase. Collagenase solution (10 mg/ml) was preheated at 37 °C for 30 min. (Collagenase was aliquoted in 5 ml tubes and stored in the freezer). In the meantime, samples were incubated in preheated 1× Hank's Balanced Salt Solution (HBSS) for 10 min at 37 °C. Incubation in collagenase solution lasted 6 h. To stop the collagenase activities, samples were briefly rinsed in 1xPBS and fixed PFA for 15 min. The fixative agent was washed 3 times for 5 min using 1xPBS. Samples were then incubated in PBST with 10 % Normal Donkey Serum (NDS) overnight as a blocking step to prevent non-specific binding of the antibodies. Sclerostin was labeled using Goat antibody prepared in PBST solution with 5 % NDS and incubated overnight at RT. Samples were then washed 3 times for 10 min in PBST followed by an overnight incubation in PBST. Secondary antibodies (Donkey anti-Goat IgG) were used and prepared in Secondary Sample Buffer with 5 % NDS. Samples were incubated for 24 h at RT. Oxazole Yellow (1:1000) was added to the secondary antibody solution for nuclear staining. Finally, samples were washed in 1xPBS overnight at RT. To guarantee labeling stability, labeled samples were incubated in 4 % PFA for 30 min at RT and washed 3 times in 1xPBS.

Negative control samples were first incubated with Isotype control Goat IgG followed by the same secondary antibodies used in the experimental conditions (Donkey anti-goat IgG).

2.5. 3D imaging

Labeled samples were immersed overnight at room temperature in EasyIndex (RI = 1.52) (LifeCanvas Technologies, Cambridge) for refractive index matching. Next, samples were mounted in 1.5 % agarose gel mixed with EasyIndex. Mounted samples were incubated in EasyIndex overnight before imaging. Images were acquired via light-sheet microscopy (SmartSpim, LifeCanvas Technologies, Cambridge) at 3.6× (1.8 µm × 1.8 µm × 2 µm voxel size) and using the following laser wavelength-emission filters combination: 488 nm - Chroma ET525/50 m, 561 nm - Chroma ET600/50 m, and 647 nm - Chroma ET690/50 m.

2.6. 3D Cell detection and cell count analysis

TIFF files containing lightsheet images were converted to Zarr files before input to an automated cell detection model (LifeCanvas Technologies, Cambridge, MA). The cell detection pipeline assessed the 3D coordinates of the detected cells' centroid. The performance of the cell detection model was compared to ground truth manual detection and detailed in previous work [16]. The F1-score was assessed to be similar to the state-of-the-art cell detection model [22]. Images were manually

segmented to isolate the cortical bone and remove any remaining external tissues or regions containing bone marrow. To normalize the sample length, the proximal and distal ends of the bone were segmented out. On the proximal end, we used the proximal tibial crest as a landmark, the region of the bone located 1 mm proximally to the tibial crest was segmented out. Bone located distally to the distal fibula tibia junction was segmented out. As a result, the region of interest analyzed is located between 15 % to 55 % of the total tibial length. Then a mask of the segmented cortical bone was generated and applied to the cell detection coordinates to exclude cells outside the cortical bone. The total cell counts were based on cell nuclei detection.

To report the number of cells along the bone length, samples were discretized in 20 μm thick sections using MATLAB (Mathworks). The number of cells detected in these sections, based on the nuclear staining, was plotted along the bone length (Fig. 3-B & 6-B).. The number of positive cells for a specific marker was determined by the ratio of cell detection in the marker channel and the total number of cells detected based on the nuclear staining (Fig. 3-C & 6-C)..

To facilitate visualization of the 3D data, the percentage of cells expressing a marker was also reported on two-dimensional surface color maps. To do so, the bone was discretized in quadrants: posterior-lateral, lateral-anterior, antero-medial, and medial-posterior (Fig. 3-D, 3-E, 6-D, 6-E). To flatten the 3D point clouds of detected cells, first a centerline was determined by calculating the centroids of 50 cross-sections along the bone. Then cells coordinates were expressed as a radial distance from the centerline and the angle between the radial vector and a reference vector. In the radial direction, the data was averaged to mimic an orthogonal projection. Coordinates were interpolated on a mesh of 300 points along the Z-axis and 200 points around the angular axis. On the 2D maps, each column corresponds to a quadrant. Samples were rotated along the centerline to guarantee a similar orientation between samples allowing location comparison. The relative change in *Sost*-positive cells between loaded and contralateral legs was reported on those 2D color maps. The relative change was calculated for each mouse by comparing the loaded leg and the corresponding contralateral leg. The relative change was then averaged into one color map.

In the literature, differences in the number of target-positive cells between experimental conditions are commonly performed in histological sections at specific locations of the bone length [7,10,12]. For comparison with the literature, we quantified the percentage of *Sost* and sclerostin-positive cells present in sections at 25, 37, 45, and 52 % of the bone length. We performed the analysis in 20 μm to 400 μm thick simulated bone cross-sections to investigate the potential influence of the selected regions on the quantification results between groups. The mean percentage of target-positive cells of each sample was plotted as individual dots (Fig. 4-A & 4-B).

In addition, we performed a comparison of the percentage of sclerostin-positive cells located specifically in the posterior-lateral region at 37 % of the bone length. Three 10 μm -thick sections per sample were analyzed. The number of cells expressing nuclear and sclerostin labeling was manually counted, as per the standard region and method for immunohistochemistry [11–13].

2.7. Statistical analysis

Statistical significance differences in the number of target-positive cells detected between loaded and contralateral groups were tested in MATLAB (open source package: spm1d.org, © T. Pataky), along the bone length, using 1D Statistical non-Parametric Mapping (SnPM1D) [23,24]. Normality tests suggested that part of the data was not normally distributed along the bone length. The SnPM1D method offers the possibility to run non-parametric tests and identify spatial changes in response to an experimental factor along the data set. Non-parametric inference takes advantage of permutation procedures described by Nichols et al. [25]. This method reduces reliance on data distribution assumptions such as normality and homoscedasticity. The null

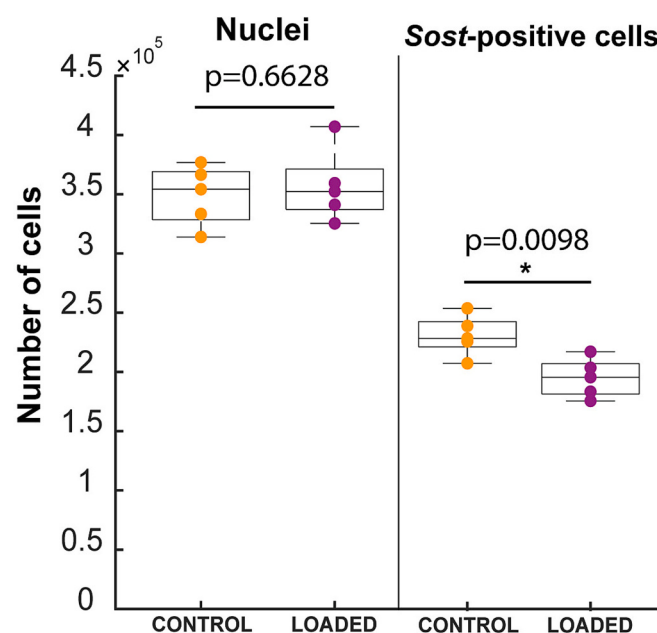


Fig. 2. Bulk cell detection analysis of contralateral ($n = 5$) and loaded ($n = 5$) samples. Bulk analysis refers to the analysis of cell detection data without considering the spatial information. Wilcoxon sum rank tests were performed to determine if the total number of cells detected was significantly different between loaded and contralateral groups for an alpha value of 0.05.

hypothesis assumed that the mean percentage of *Sost*-positive or sclerostin-positive cells is equivalent between loaded and contralateral groups, for $\alpha = 0.05$. SnPM1D test results are presented as SnPM{t} curves along the tibial region of interest for each experimental condition. Red dotted lines indicate the critical thresholds (noted t^*) beyond which the null hypothesis is rejected at a Type I rate of $\alpha = 0.05$ (Supplements Figs. 3 & 4). Statistical analysis was performed to test significant differences in the number of *Sost*-positive cells ($n = 5$ mice, 2 bones per mouse: loaded and control, $\sim 350,000$ cells per bone sample on average) and sclerostin-positive cells ($n = 5$ mice, 2 bones per mouse: loaded and control, $\sim 380,000$ cells per bone sample on average), between loaded and control legs.

For comparison with the literature, we statistically tested for significant differences, between loaded and contralateral groups, at 25, 37, 45, and 52 % of the bone length using the Wilcoxon sum rank test, for $\alpha = 0.05$. The null hypothesis assumed that the mean percentage of cells expressing the target at the tested location is equal between loaded and contralateral groups. These regions specific analyses were performed for both *Sost*-positive ($n = 5$ mice, 2 bones/mouse, ~ 1000 cells/ 20- μm -section, $\sim 15,500$ cells/ 400- μm -section) and sclerostin-positive osteocytes ($n = 5$ mice, 2 bone/mouse, ~ 1000 cells/20- μm -section, $\sim 17,000$ cells/400- μm -section).

Similarly, the Wilcoxon sum rank test ($\alpha = 0.05$) was used to test differences in the manually counted percentage of sclerostin-positive cells in the posterior-lateral region, between loaded and contralateral groups ($n = 5$ mice, 2 bones per mouse: loaded and control, 3 sections per bone, ~ 60 cells analyzed per section on average, for a total of ~ 1900 cells analyzed).

3. Results

In this work, we investigated the spatial regulation of *Sost* gene expression and sclerostin protein expression in osteocytes following in vivo tibia loading. To do so, we used the recently published WISH-BONE method [16] and uniaxial tibia loading [1,2]. Investigating the spatial change in osteocytes expressing *Sost* mRNA transcripts indicates the early biological response to compressive loading while expression of

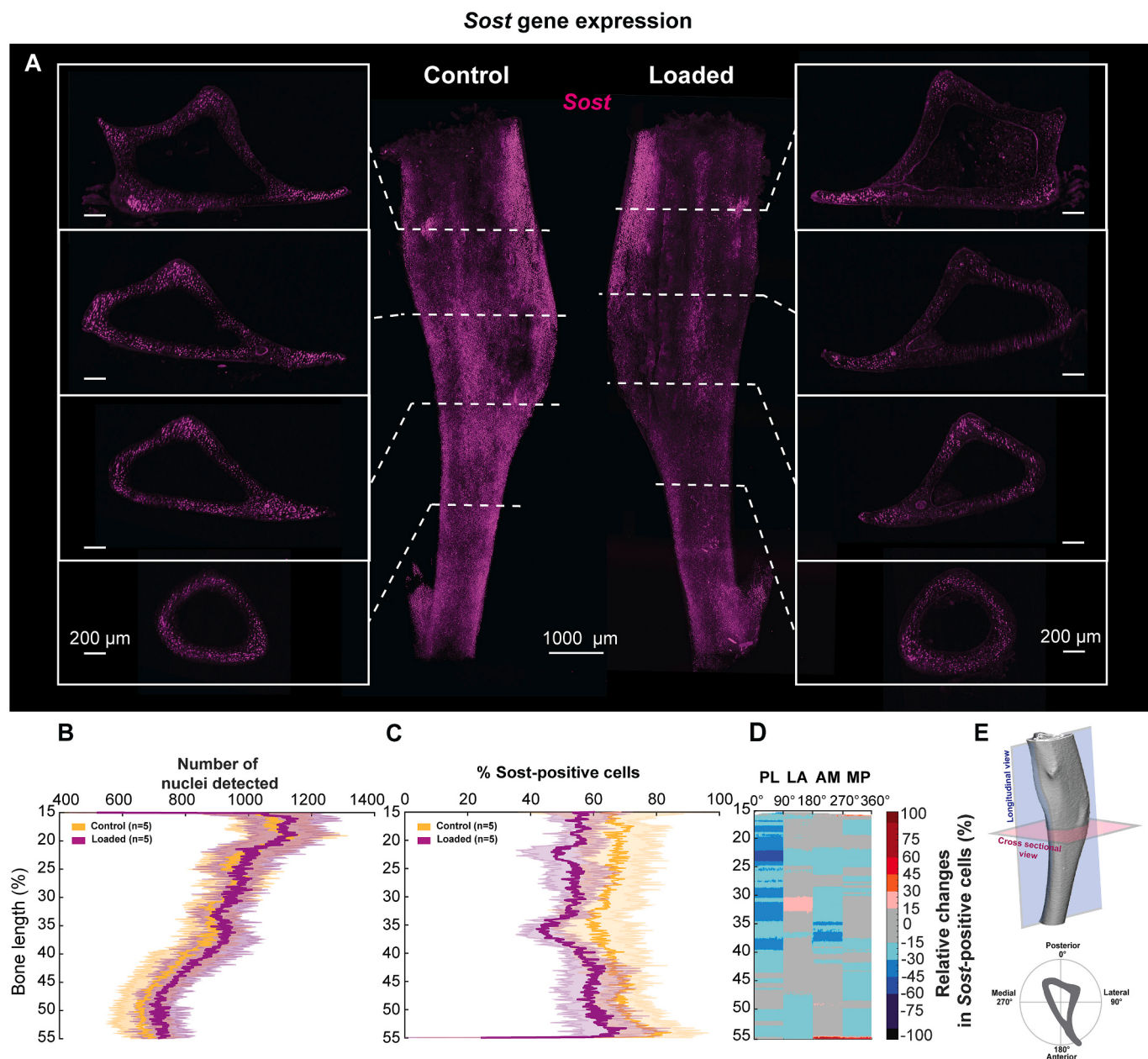


Fig. 3. Spatial investigation for *Sost* mRNA expression in loaded vs contralateral legs. A) Lightsheet images of a representative contralateral and loaded mouse tibia midshafts labeled for *Sost* mRNA using HCR-FISH. The scale bar of the insets represents 200 μ m. B) Comparison between loaded and contralateral legs ($n = 5$) of the total number of cells detected based on nuclear staining along the bone length. Bold lines present the mean percentage of *Sost*-positive cells and shaded bands indicate standard deviation. C) Percentage of *Sost*-positive cells along the bone length of loaded and contralateral legs ($n = 5$). D) 2D heat map showing the relative change in *Sost*-positive cells between loaded and contralateral leg along the bone length and within each bone quadrant (PL: Posterior-Lateral, LA: Lateral-Anterior, Anterior-Medial, Medial-Posterior). A negative relative change suggests a decrease in the percentage of *Sost*-positive cells in the loaded leg compared to the contralateral leg ($n = 5$). E) Illustration showing the orientation of the longitudinal plan and cross-sectional plan in the tibia. It also shows the definition of the cross-sectional quadrants used for the 2D heat map.

sclerostin protein provides a downstream (later in time) response.

3.1. 3D investigation of *Sost*-positive osteocytes reveals significant decrease after loading

We first performed a bulk analysis of the 3D *Sost* mRNA labeling by considering all the cells detected in the entire sample as one data set. Bulk analysis showed a total number of cells detected based on nuclear staining of about 350,000 cells on average per sample. A similar total number of cells was detected between the loaded and contralateral samples. The average percent difference in detected nuclei was 2 %

between conditions, which was not significantly different. However, the total number of cells detected as *Sost*-positive was significantly lower in loaded tibiae compared to contralateral tibiae ($p < 0.01$) (Fig. 2), with a 17 % difference.

Fig. 3-A shows the 3D reconstruction of the lightsheet images for both contralateral and loaded legs labeled for *Sost* mRNA transcripts. Similar to the bulk analysis, the total number of cells was found to be similar along the bone length between both groups (Fig. 3-B). The percentage of positive cells was defined by the ratio of the number of cells expressing *Sost* to the number of nuclei in the cortical bone. We observed between 55 % and 65 % of the cells expressing *Sost* mRNA transcripts along the

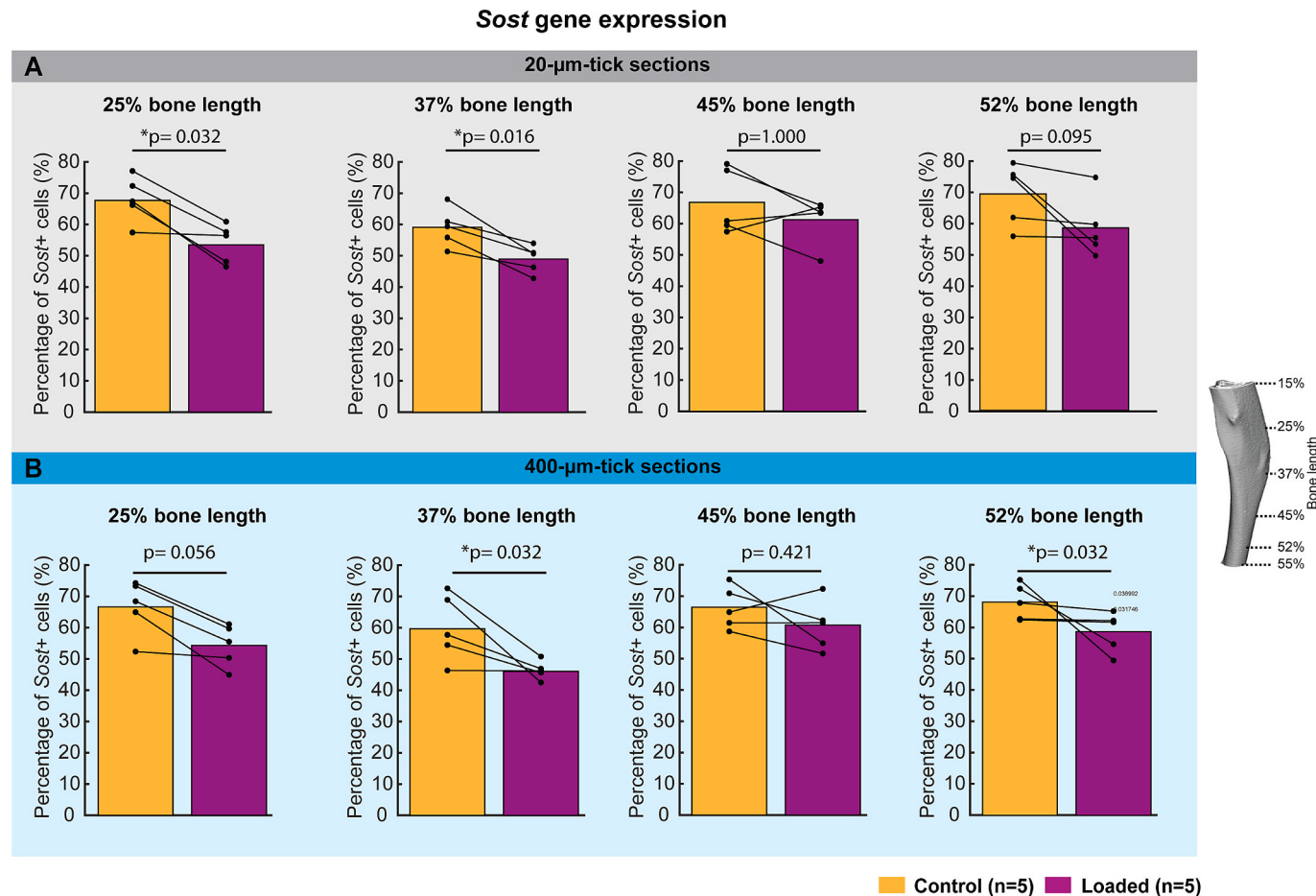


Fig. 4. Region-specific statistical analysis of *Sost*-positive cells in loaded ($n = 5$) and contralateral ($n = 5$) samples. A) Percentage of *Sost*-positive cells detected within 20 μm thick cross-section located at 25 %, 37 %, 45 %, and 52 % of the bone length in both groups. Wilcoxon sum rank tests showed a significant difference between loaded and contralateral legs at 25 % and 37 % of the bone length ($\alpha = 0.05$). Black lines connect loaded and contralateral legs of the same mouse. B) Percentage of *Sost*-positive cells detected within 400 μm thick cross-section located between 25–27 %, 35–37 %, 45–47 %, and 51–53 % of the bone length in both groups. Statistical tests showed a significant difference between loaded and contralateral legs in the regions 35–37 % and 51–53 % ($\alpha = 0.05$). * : p-values < 0.05

tibia length in both groups. Comparison with negative control ($n = 1$) showed only 2 % of the cells expressing non-specific signal, indicating our labeling is specific for *Sost* (Supplements Figure-1). Figs. 3-C & 3-D show the result of the spatial analysis and the number of *Sost*-positive cells along the bone length. We observed a drop in *Sost*-positive cells in the loaded legs compared to contralateral legs between 20 and 25 % and 35–40 % of the tibia length, which are typical regions of adaptation reported in the literature [5,7,9,13]. SnPM1D analysis was conducted along the length of the samples to test for statistical significance between loaded and contralateral groups. SnPM1D is a statistical analysis that takes into account the data along the bone length; thus, this test is less sensitive to localized changes between conditions. SnPM1D results did not show statistical differences for an α -value of 0.05 (Supplemental Fig. 3), suggesting that the changes might be localized. However, when considering bone cross-section of 20 μm , Wilcoxon sum rank tests showed a significant decrease of *Sost*-positive cells at 25 % and 37 % of the bone length between loaded and contralateral leg (α -value = 0.05). In 400 μm thick sections, statistical tests showed significant differences between loaded and contralateral groups at 37 % and 52 % of the bone length, whereas the region at 25 % of the bone length was not significantly different ($p = 0.056$). These results suggest that the region selected for analysis influences the measurement and could alter the interpretation of the results. These results suggest that statistical analysis might lead to different conclusions depending on the region of the bone considered for analysis and the utilized methods.

The 2D colored map showed the relative changes in the percentage of

Sost-positive cells in the 3D samples (Fig. 3-D). A negative relative change suggests a decrease in the number of cells expressing *Sost* in the loaded legs compared to the contralateral legs. We observed that most of the decrease in relative change happened in the posterior-lateral side of the bone, where several regions along the bone length presented a decrease in *Sost*-positive cells of 30 % or higher compared to contralateral tibiae. The posterior-lateral side of the bone is where the mechanical stimuli are known to be the highest (strain magnitude [7,26], fluid flow velocity [9,27], etc.).

3.2. 3D distribution of sclerostin-positive osteocytes is similar between loaded and control tibia

Sost is a gene encoding for the protein sclerostin. As a second step, we aimed to investigate the spatial regulation of sclerostin protein in the mouse tibia following loading. Following the same approach, we analyzed sclerostin protein expression in osteocytes along the bone length after two weeks of loading.

Bulk analysis of the whole-mount sclerostin protein labeling showed a similar number of total cells detected in both groups (1.5 % difference) based on nuclear staining. Similarly, the percent difference in the number of sclerostin-positive cells detected in loaded and contralateral groups was not significant (1 %). A total of about 380,000 cells on average were detected per sample based on the nuclear staining and about 225,000 cells were detected as sclerostin-positive on average (Fig. 5).

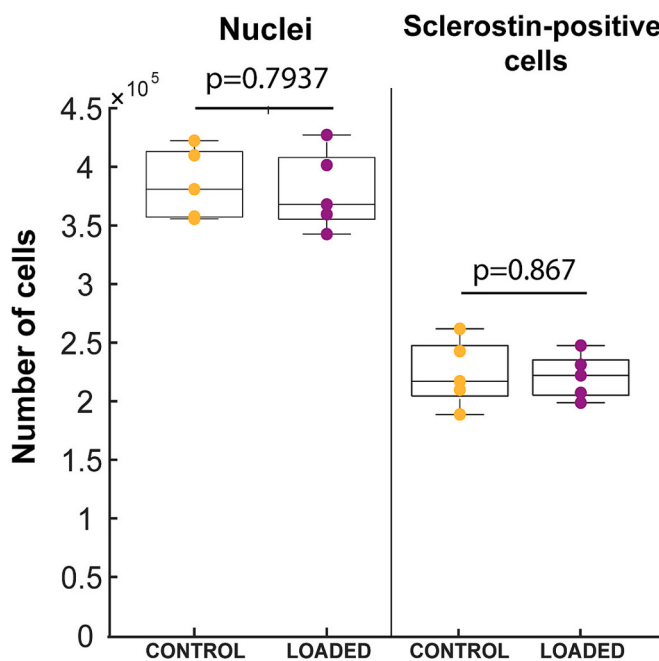


Fig. 5. Bulk cell detection analysis of contralateral ($n = 5$) and loaded ($n = 5$) samples. Bulk analysis refers to the analysis of cell detection data without considering the spatial information. Wilcoxon sum rank tests ($\alpha = 0.05$) were performed to determine if the number of cells detected was significantly different between loaded vs contralateral groups.

Fig. 6-A presents the 3D reconstruction of a loaded and control mouse tibia midshaft labeled for sclerostin. Spatially, we detected a similar number of cells based on nuclei staining along the bone length (**Fig. 6-B**). We observed about 60 % of the cells expressing sclerostin along both contralateral and loaded legs (**Fig. 6-C**). Whereas the percentage of cells presenting non-specific fluorescence, in negative controls, was below 7 % (Supplemental Fig. 2). The analysis of the sclerostin-positive cells did not show drops in the number of positive cells along the bone in the loaded compared to contralateral tibia midshafts (**Fig. 6-C**).

The analysis around the bone cross-section, presented as a 2D colored map (**Fig. 6 - D**), did not exhibit a region of change of $>30\%$. A few regions had a decrease in the relative change between loaded and contralateral legs of around 15 %. Those regions were located around 37 % and 50 % of the bone length, mostly on the posterior-lateral and anteromedial, similar to the *Sost* gene expression analysis. However, the change in the percentage of sclerostin-positive cells was mild compared to the mRNA analysis.

SnPM1D tests showed that the loaded and control groups were not significantly different in terms of the percentage of sclerostin-positive cells along the bone length, for $\alpha = 0.05$ (Supplemental Fig. 4). Similar results were found during sections analysis at 25 %, 37 %, 45 %, and 52 % of the bone length in 20 μm -thick (**Fig. 7-A**) and 400 μm -thick cross-sections (**Fig. 7-B**).

In the literature, histological analysis of thin 2D sections is used to quantify the number of target-positive osteocytes in the cortical bone between experimental conditions. Here we mimicked this histological approach and quantified the percentage of sclerostin-positive cells in the posterior-lateral region at 37 % of the bone length, for both loaded and contralateral samples (**Fig. 8**). **Fig. 8-A** presents an example of 2D sections, from the 3D data set, and highlights the posterior-lateral regions that were quantified. Using this method, we quantified an average decrease of 18 % in the loaded group compared to contralateral (**Fig. 8-B**). The percentage of sclerostin-positive cells was found to be significantly different at this location ($\alpha = 0.05$).

4. Discussion

In this study, we used the 3D mRNA and protein labeling methods, WISH-BONE, to investigate the spatial regulation of sclerostin protein expression and the encoding gene, *Sost*, following *in vivo* tibia loading. Using our spatial analysis, we showed that the method captured a decrease in the percentage of osteocytes expressing *Sost* mRNA transcripts in the loaded group compared to the contralateral group. Decreases in the percentage of *Sost*-positive osteocytes were measured mostly around 25 % and 37 % of the bone length, which are known to be regions of adaptation [5,9] (**Fig. 3-C**), and in the posterior-lateral side of the tibia where the mechanical stimulus is known to be the highest under uniaxial compression [7–9,27] (**Fig. 3-D**). We investigated the percentage of sclerostin-positive cells in the tibia after two weeks of loading. This loading protocol has been shown to induce bone adaptation in mature mouse bone [7,9,26,28]. We found that the percentage of osteocytes expressing the protein sclerostin was similar along the bone length in both experimental conditions. However, significant differences could be found between loaded and contralateral groups when only considering the posterior-lateral region at 37 % of the bone length and three 10 μm -thick sections per sample.

Previous work investigating the regulation of *Sost* gene expression following mechanical stimulation reported a decrease in *Sost* gene expression in the loaded samples compared to controls. Using methods such as RT-PCR, studies showed a downregulation by 50 % of the *Sost* gene expression 4 h and 24 h after loading compared to control legs [6]. In 2D histological sections of the ulna, the expression of *Sost* was also suggested to decrease by 50 % in regions experiencing high magnitude of mechanical stimulation [12]. Chlebek et al. used RNA-seq and In Situ Hybridization in mouse tibiae. They reported a 2-fold change or higher of *Sost* in the tibia mid-diaphysis experiencing high magnitude of mechanical stimuli, 24 h after loading [14]. In these previous studies, the method utilized required homogenization of the sample or 2D sectioning which limit the spatial investigation of gene regulation. In the present study, we reported a downregulation of the *Sost* gene expression 24 h after the first loading bout, which is consistent with the literature. In addition, we provided 3D spatial information regarding the location of this downregulation. We found that most of the reduction in *Sost*-positive osteocytes occurred in the posterior-lateral region of the tibia midshaft, where the magnitude of the mechanical stimuli is known to be the highest during uniaxial tibia compression [7–9].

We investigated the regulation of the sclerostin protein in osteocytes in 3D mouse tibia after two weeks of loading. The loading protocol we used has been commonly used in mouse adaptation studies and is known to lead to bone adaptation in adult mouse bones [7,9,10,17]. After two weeks of loading, mouse tibia has been shown to still actively bone using histomorphometry [17,26]. However, it was unclear if the expression of sclerostin protein would be sustained in 3D mouse tibia after the two weeks of loading. Our 3D analysis showed that the percentage of sclerostin-positive osteocytes was similar in loaded and contralateral groups, which differs from previous histological results investigating sclerostin regulation 24 h after 2 consecutive days of loading [7,12,13,19]. In our experiment, tibiae were collected 15 days after the start of the loading protocol and 3 days after the last loading session. At this time point, sclerostin protein expression might have returned to baseline in osteocytes. In a previous study, Robling et al. reported, in 2D cross-sections, a larger decrease of sclerostin-positive osteocytes in region of the ulna experiencing higher mechanical stimuli [12]. Results suggested a decrease of about 50 % in sclerostin positive cells for a deformation of 2000 microstrain, 24 h after 2 days of loading. Later, another group showed that the percentage of sclerostin-positive cells, counted in mouse ulna 2D cross-sections, decreases by 50 % 24 h after loading (~ 2200 microstrain), before returning to baseline 48 h after a single loading session [19]. Similar results were found by Meakin et al. in the posterior-lateral side of mouse tibia midshaft at 37 % of the bone length [10], where the mechanical stimulation is known to be the

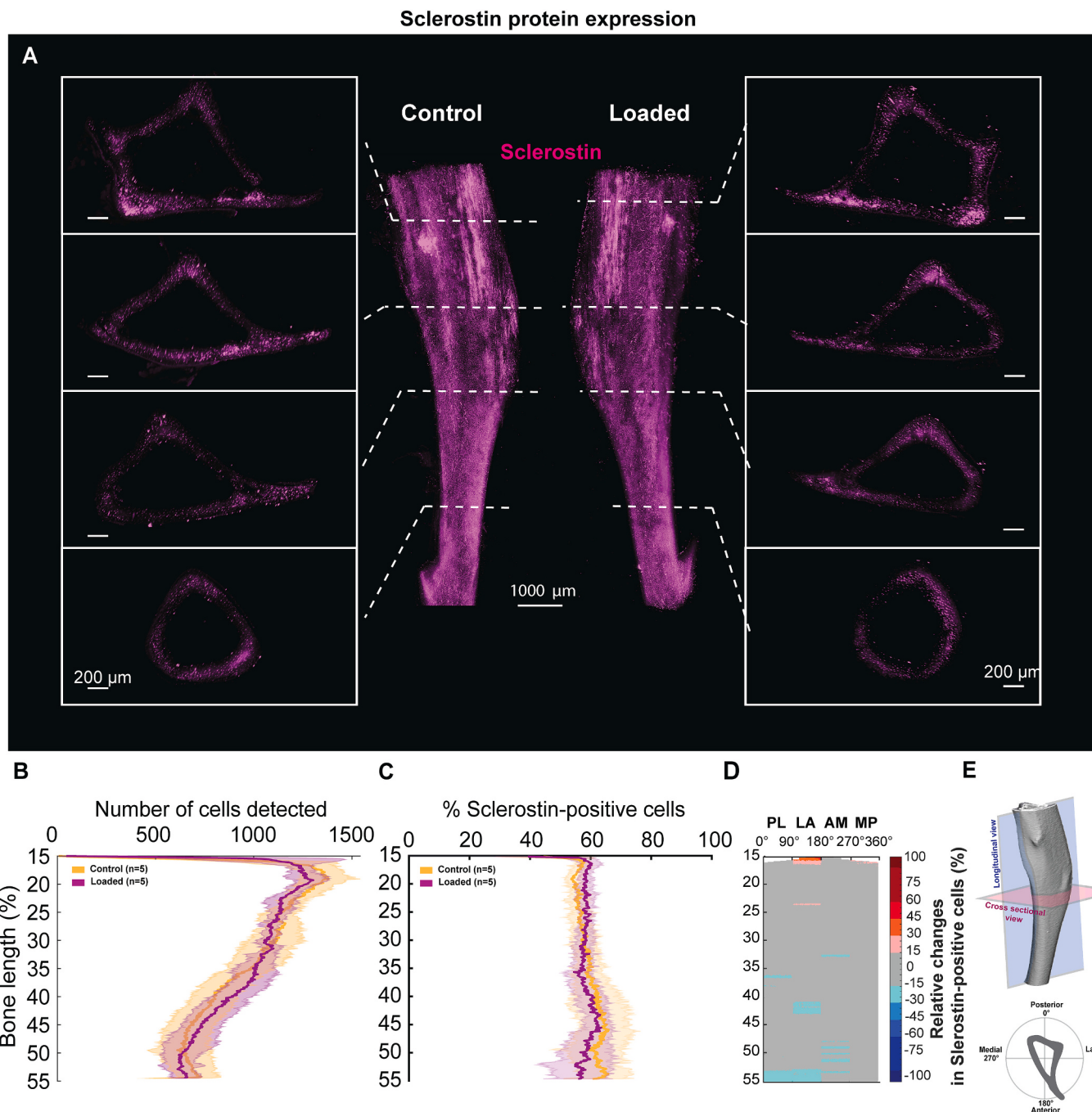


Fig. 6. Spatial investigation for Sclerostin expression in loaded vs contralateral legs. A) Lightsheet images of contralateral and loaded mouse tibia midshafts labeled for Sclerostin using whole-mount immunolabeling. B) Comparison between loaded ($n = 5$) and contralateral ($n=5$) legs of the total number of cells detected based on nuclear staining along the bone length. C) Percentage of Sclerostin-positive cells along the bone length of loaded and contralateral legs. D) 2D heat map showing the relative change in Sclerostin-positive cells between loaded and contralateral leg along the bone length and within each bone quadrant (PL: Posterior-Lateral, LA: Lateral-Anterior, AM: Anterior-Medial, MP: Medial-Posterior). A negative relative change suggests a decrease in the percentage of Sclerostin-positive cells in the loaded compared to contralateral legs. E) Illustration showing the plan the orientation of the longitudinal plan and cross-sectional plan in the tibia. It also shows the definition of the cross-sectional quadrants used for the 2D heat map.

highest. In addition, Holguin et al. found a decrease of about 20 % in the number sclerostin-positive osteocytes 24 h after loading, in the posterior-lateral side of 2D mouse tibia cross-sections, when using a target strain of 2200 macrostrain [13]. However, the number of sclerostin-positive osteocytes was similar in loaded and contralateral groups after 5 days of loading, suggesting a return to baseline of the sclerostin expression. Another study by Gould et al. [29] showed that the downregulation of sclerostin happened 5 min after loading, using the ulna loading model.

Together, these results suggest that the time point of sample collection used in our study (3 days after the last loading session) might have allowed the sclerostin expression to return to baseline.

However, we measured a downregulation of *Sost* gene expression using the same loading magnitude, which suggests that the loading profile had the intended biological effects and supports the hypothesis of late timing for the protein analysis. In addition, when simulating 2D immunohistochemistry, we found a local significant decrease in the number sclerostin-positive cells after loading at 37 % of the bone length

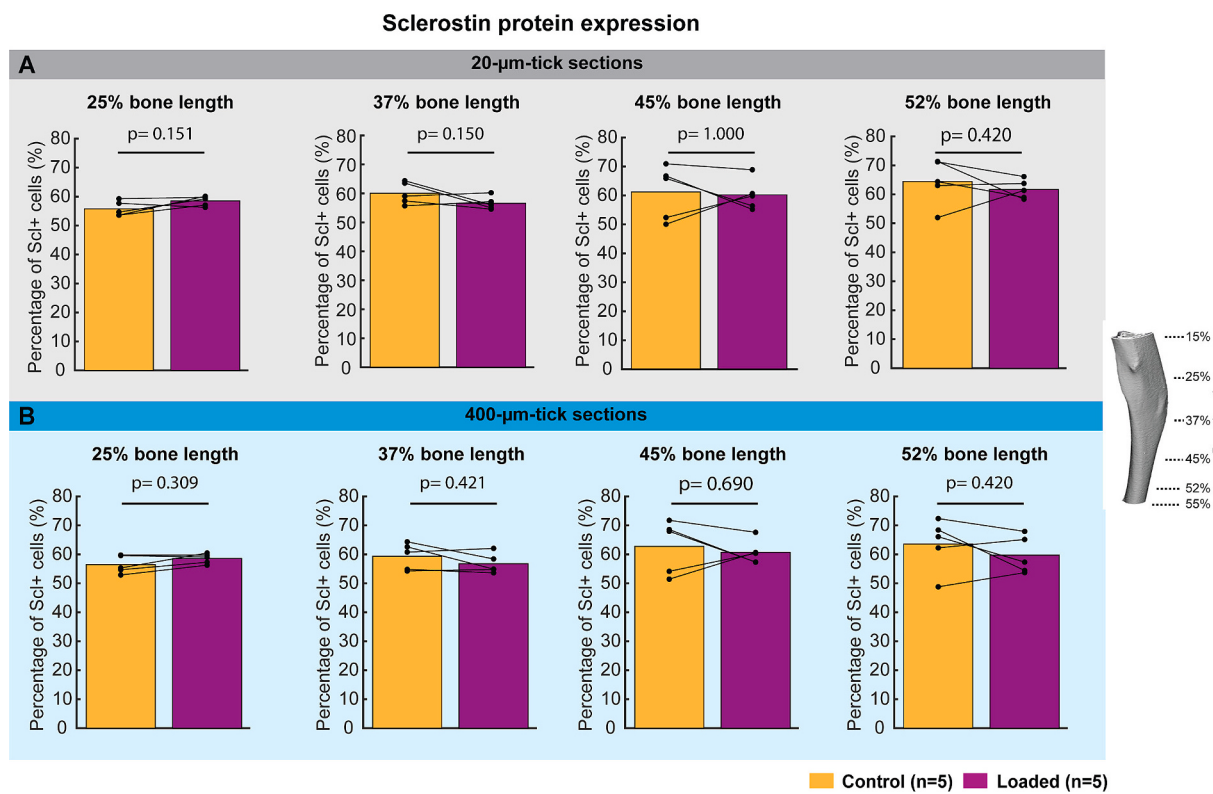


Fig. 7. Region-specific statistical analysis of Sclerostin-positive cells. A) Percentage of Sclerostin-positive cells detected within 20 μm thick cross-section located at 25 %, 37 %, 45 %, and 52 % of the bone length in both groups. Solid lines indicate samples from the same mouse. Statistical analysis did not show a significant difference between loaded ($n = 5$) and contralateral ($n = 5$) legs at the tested location ($\alpha = 0.05$). B) Percentage of Sclerostin-positive cells detected within 400 μm thick cross-section located between 25–27 %, 35–37 %, 45–47 %, and 51–53 % of the bone length in both groups. No significant difference between loaded and contralateral legs was detected ($\alpha = 0.05$).

(Fig. 8).

In our study, we used 2D histological-like approach and quantified the number of sclerostin-positive cells in the posterior-lateral side of 2D mouse tibia cross-section, we found a significant decrease of 18 % after loading. These results better capture previous results from the literature reported above. These results could suggest a highly localized downregulation of sclerostin protein expression or a lack of representativity of 2D sections to capture the response of the entire 3D sample.

Other studies showed that the repetition of multiple loading cycles and loading sessions is necessary to trigger a bone adaptation response [5,30] and to obtain a measurable amount of bone formation. In addition, 2 weeks of uniaxial tibia loading has been suggested to have long-term/chronic effects on mouse tibia morphology [31] which might have suggested a sustained downregulation of sclerostin protein in this loading protocol. Because typical histological results quantifying sclerostin-positive cells only focused on thin bone sections at specific location of the bone; one could have hypothesized that sustained downregulation of sclerostin might have been missed at other locations of the bone. Here we reported no changes in percentage of sclerostin-positive osteocytes in the entire 3D tibia midshaft, after two weeks of loading (6 loading sessions of 100 cycles), which suggests the lack of sustained effect of the loading protocol on the downregulation of sclerostin protein expression in osteocytes.

The potential limitation of this approach is that our labeling and cell detection model might prevent capturing slight downregulation of sclerostin expression in individual cells. A small change in sclerostin protein expression may result in a minor change in fluorescence due to the amplification of the signal through secondary antibodies. These slightly less bright cells might still be bright enough to be detected in our current detection pipeline, preventing assessment of the level of expression. Less sensitive cell detection models could be trained to

investigate this question.

Although the WISH-BONE method allows the investigation of hundreds of thousands of cells per sample, the number of samples per condition, in this study, is small ($n = 5$ per condition). The sample size was limited by the large image size (50 GB to 100 GB) and the manual segmentation required to isolate the cortical bone.

We have shown equivalence of our method to 2D immunohistochemistry by isolating, from our 3D data sets, thin 2D sections in the standard region of analysis (37 % bone length) and counting the number of sclerostin-positive cells in the posterior-lateral side of the tibia. We demonstrated in this very isolated region a downregulation of sclerostin, consistent with the literature. We did not investigate other locations around the 2D sections such as the anterior-medial side which is under tension during tibia loading. In this study, we simulated 2D immunohistochemistry using our 3D data sets but we did not separately perform traditional 2D immunohistochemistry.

The WISH-BONE method does not currently allow the use of the same sample for microCT analysis or histomorphometry and 3D fluorescent labeling. Future efforts will optimize WISH-BONE protocol to allow microCT scanning and 3D labeling in the same bones, which will inform about molecular expression and bone formation in the same 3D mouse bone sample.

In this work, we highlight the importance of carefully selecting the region of interest and the influence of the method chosen for its analysis. The 2D color maps (Fig. 3-D & 6-D) allow the investigation of molecular regulation around the entire bone cross-section and provide further detail on the spatial location of the regulation compared to simply running the analysis in bulk or along the length of the bone. This method also enables potential correlation between mechanical environments and molecular expression changes [9]. Despite the similarities of the 3D Sclerostin protein data set between loaded and contralateral groups

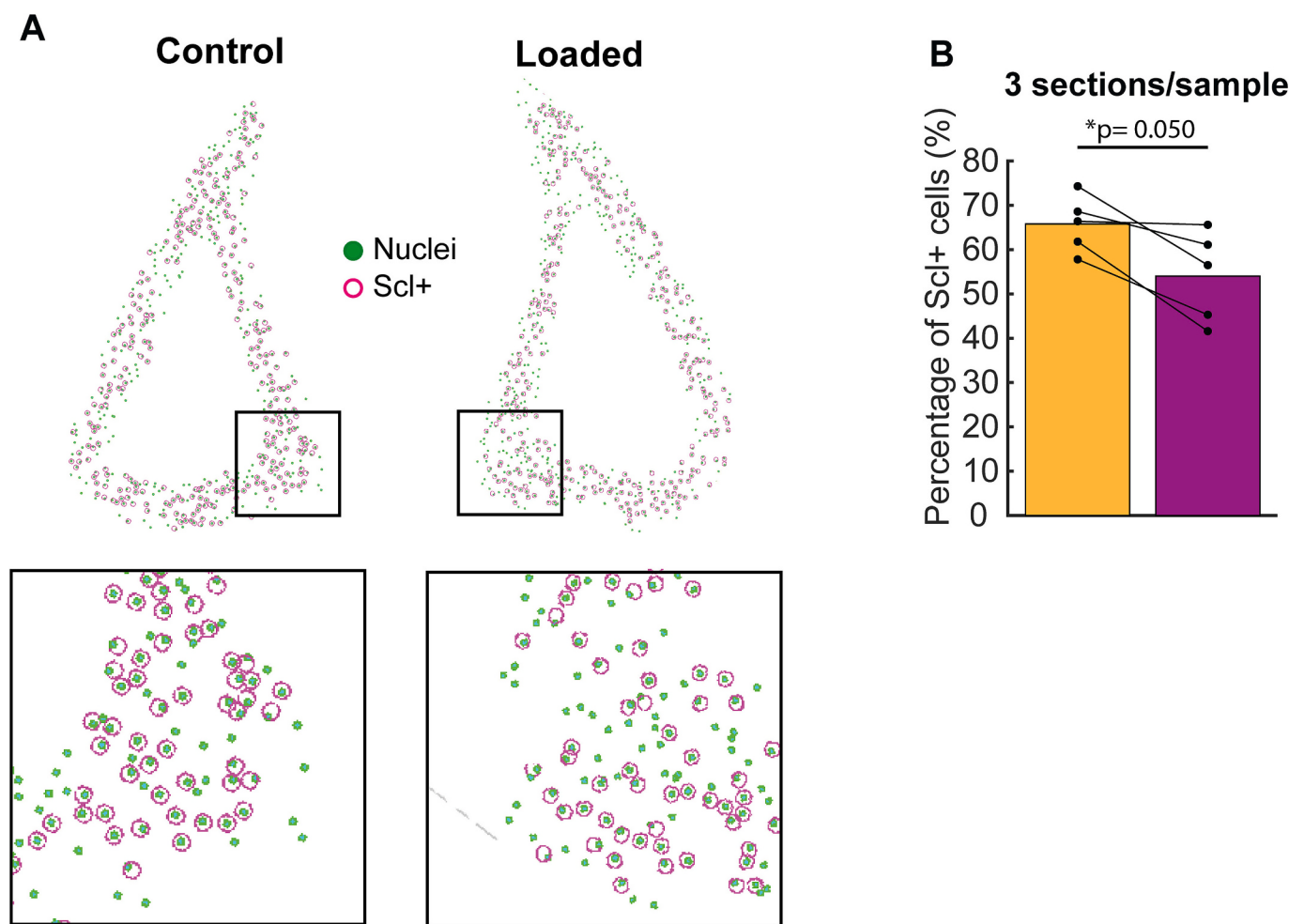


Fig. 8. Histological analysis of the loaded ($n = 5$) and contralateral ($n = 5$) bones. A) Simulated tibia cross-sections from loaded and contralateral legs based on 3D lightsheet data. Analyzed sections were localized at 37 % of the bone length. Cells located in the posterior-lateral regions (insets) of the sections were manually counted and the percentage of cells expressing sclerostin (Scl^+) was reported. B) Results were reported after analysis of three consecutive $10 \mu\text{m}$ -thick sections per sample. Analysis was conducted using the 3D cell detection data from the lightsheet images.

(Figs. 5,6,7), we found statistically significant differences in the posterior-lateral region at 37 % of the bone between our groups (Fig. 8). At this location, three $10 \mu\text{m}$ -thick sections per sample were analyzed, as commonly performed in the literature. We measured a decrease of about 18 % in sclerostin-positive cells. These results highlight the influences of the method of analysis on the interpretation of the effect of the mechanical loading used.

5. Conclusions

In this work, we investigated the 3D distribution of *Sost* mRNA and sclerostin protein expression in osteocytes respectively after 24 h and 2 weeks of uniaxial tibia compression. The new WISH-Bone method provides important information on the location of the downregulation of *Sost* in 3D. The protein analysis emphasized the influence of the methods and locations of quantification of sclerostin-positive cells on the interpretation of the mechanoadaptation response. Investigating abundantly expressed genes and proteins in 3D should provide a better understanding of the mechanoadaptation response in healthy and pathological bones.

CRediT authorship contribution statement

Quentin A. Meslier: Writing – review & editing, Writing – original draft, Visualization, Methodology, Investigation, Formal analysis,

Conceptualization. **Jacy Hoffmann:** Formal analysis. **Robert Oehrlein:** Formal analysis. **Daniel Kurczy:** Formal analysis. **James R. Monaghan:** Writing – review & editing, Supervision, Methodology, Funding acquisition, Conceptualization. **Sandra J. Shefelbine:** Writing – review & editing, Supervision, Methodology, Funding acquisition, Conceptualization.

Declaration of competing interest

The authors declare the following financial interests/personal relationships which may be considered as potential competing interests:

Quentin A. Meslier reports equipment, drugs, or supplies was provided by Lifecanvas Technologies. Quentin A. Meslier was interning at LifeCanvas Technologies as part of a NSF INTERN supplement. Sandra J. Shefelbine serves in the editorial board of the following journals: *J. Biomech.*; *Bone*. If there are other authors, they declare that they have no known competing financial interests or personal relationships that could have appeared to influence the work reported in this paper.

Acknowledgments

This work was funded by the National Science Foundation CMMI # 2010010 and the National Science Foundation INTERN supplement.

We thank the Institute for Chemical Imaging of Living Systems (RRID:[SCR_022681](#)) at Northeastern University for consultation and

instrument support.

In addition, we thank LifeCanvas technology for their guidance in tissue labeling and imaging.

Appendix A. Supplementary data

Supplementary data to this article can be found online at <https://doi.org/10.1016/j.bone.2025.117422>.

Data availability

Examples of 3D images acquired using lightsheet microscopy are available on the following repository: <https://hdl.handle.net/2047/D20695830>.

References

- [1] J. Fritton, E. Myers, T. Wright, M. Vandermeulen, Loading induces site-specific increases in mineral content assessed by microcomputed tomography of the mouse tibia, *Bone* 36, no. 6, Art. no. 6 (2005), <https://doi.org/10.1016/j.bone.2005.02.013>.
- [2] R.L. De Souza, M. Matsuura, F. Eckstein, S.C.F. Rawlinson, L.E. Lanyon, A. Pitsillides, Non-invasive axial loading of mouse tibiae increases cortical bone formation and modifies trabecular organization: a new model to study cortical and cancellous compartments in a single loaded element, *Bone* 37, no. 6, Art. no. 6 (2005), <https://doi.org/10.1016/j.bone.2005.07.022>.
- [3] Y.-F. Hsieh, A.G. Robling, W.T. Ambrosius, D.B. Burr, C.H. Turner, Mechanical loading of Diaphyseal bone in vivo: the strain threshold for an osteogenic response varies with location, *J. Bone Miner. Res.* 16 (12) (2001) 2291–2297, <https://doi.org/10.1359/jbmr.2001.16.12.2291>.
- [4] R.P. Main, S.J. Shefelbine, L.B. Meakin, M.J. Silva, M.C.H. Meulen, B.M. Willie, Murine axial compression Tibial loading model to study bone Mechanobiology: implementing the model and reporting results, *J. Orthop. Res.* 38, no. 2, Art. no. 2 (2020), <https://doi.org/10.1002/jor.24466>.
- [5] H. Yang, R. E. Embry, and R. P. Main, “Effects of Loading Duration and Short Rest Insertion on Cancellous and Cortical Bone Adaptation in the Mouse Tibia,” *PLoS ONE*, vol. 12, no. 1, Artery 1, Jan. 2017, doi:<https://doi.org/10.1371/journal.pone.0169519>.
- [6] N. Holguin, M.D. Brodt, M.J. Silva, Activation of Wnt signaling by mechanical loading is Impaired in the bone of old mice: LOAD-INDUCED ACTIVATION OF WNT SIGNALING IMPAIRED IN BONE OF OLD MICE, *J. Bone Miner. Res.* 31 (12) (2016) 2215–2226, <https://doi.org/10.1002/jbmr.2900>.
- [7] A. Moustafa, et al., Mechanical loading-related changes in osteocyte sclerostin expression in mice are more closely associated with the subsequent osteogenic response than the peak strains engendered, *Osteoporos. Int.* 23 (4) (2012) 1225–1234, <https://doi.org/10.1007/s00198-011-1656-4>.
- [8] H. Razi, et al., Skeletal maturity leads to a reduction in the strain magnitudes induced within the bone: a murine tibia study, *Acta Biomater.* 13 (2015) 301–310, <https://doi.org/10.1016/j.actbio.2014.11.021>.
- [9] Q.A. Meslier, N. DiMauro, P. Somanchi, S. Nano, S.J. Shefelbine, Manipulating load-induced fluid flow in vivo to promote bone adaptation, *Bone* 165 (2022) 116547, <https://doi.org/10.1016/j.bone.2022.116547>.
- [10] L.B. Meakin, G.L. Galea, T. Sugiyama, L.E. Lanyon, and J.S. Price, “Age-Related Impairment of Bones’ Adaptive Response to Loading in Mice Is Associated With Sex-Related Deficiencies in Osteoblasts but Not Change in Osteocytes: AGE-RELATED IMPAIRMENT OF BONES’ ADAPTIVE RESPONSE TO MECHANICAL LOADING,” *J Bone Miner Res.* vol. 29, no. 8, Artery 8, Aug. 2014, doi:<https://doi.org/10.1002/jbmr.2222>.
- [11] A. Moustafa, et al., The mouse fibula as a suitable bone for the study of functional adaptation to mechanical loading, *Bone* 44 (5) (2009) 930–935, <https://doi.org/10.1016/j.bone.2008.12.026>.
- [12] A.G. Robling, et al., Mechanical stimulation of bone in vivo reduces osteocyte expression of Sost/Sclerostin, *J. Biol. Chem.* 283, no. 9, Art. no. 9 (2008), <https://doi.org/10.1074/jbc.M705092200>.
- [13] N. Holguin, M.D. Brodt, M.J. Silva, Activation of Wnt signaling by mechanical loading is Impaired in the bone of old mice: LOAD-INDUCED ACTIVATION OF WNT SIGNALING IMPAIRED IN BONE OF OLD MICE, *J. Bone Miner. Res.* 31 (12) (2016) 2215–2226, <https://doi.org/10.1002/jbmr.2900>.
- [14] C. Chlebek, J. A. Moore, F. P. Ross, and M. C. H. van der Meulen, “Molecular identification of spatially distinct anabolic responses to mechanical loading in murine cortical bone,” *J. Bone Miner. Res.*, p. jbmr.4686, Sep. 2022, doi:<https://doi.org/10.1002/jbmr.4686>.
- [15] N.H. Kelly, J.C. Schimenti, F.P. Ross, M.C.H. Van Der Meulen, Transcriptional profiling of cortical versus cancellous bone from mechanically-loaded murine tibiae reveals differential gene expression, *Bone* 86 (2016) 22–29, <https://doi.org/10.1016/j.bone.2016.02.007>.
- [16] Q.A. Meslier, T.J. Duerr, B. Nguyen, J.R. Monaghan, S.J. Shefelbine, WISH-BONE: whole-mount *in situ* histology, to label osteocyte mRNA and protein in 3D adult mouse bones, Mar 15 (2024), <https://doi.org/10.1101/2024.03.14.585053>.
- [17] J. Piet, D. Hu, R. Baron, S.J. Shefelbine, Bone adaptation compensates resorption when sciatic neurectomy is followed by low magnitude induced loading, *Bone* 120 (2019) 487–494, <https://doi.org/10.1016/j.bone.2018.12.017>.
- [18] H. Razi, A.I. Birkhold, R. Weinkamer, G.N. Duda, B.M. Willie, S. Checa, Aging leads to a dysregulation in mechanically driven bone formation and resorption, *J. Bone Miner. Res.* 30 (10) (2015) 1864–1873, <https://doi.org/10.1002/jbmr.2528>.
- [19] N. Lara-Castillo, et al., In vivo mechanical loading rapidly activates β -catenin signaling in osteocytes through a prostaglandin mediated mechanism, *Bone* 76 (2015) 58–66, <https://doi.org/10.1016/j.bone.2015.03.019>.
- [20] A. M. Lovely, T. J. Duerr, D. F. Stein, E. T. Mun, and J. R. Monaghan, “Hybridization Chain Reaction Fluorescence *In Situ* Hybridization (HCR-FISH) in *Ambystoma mexicanum* Tissue,” in *Salamanders*, vol. 2562, A. W. Seifert and J. D. Currie, Eds., in *Methods in Molecular Biology*, vol. 2562, , New York, NY: Springer US, 2023, pp. 109–122. doi:https://doi.org/10.1007/978-1-0716-2659-7_6.
- [21] H. M. T. Choi et al., “Third-generation *in situ* hybridization chain reaction: multiplexed, quantitative, sensitive, versatile, robust,” *Development*, vol. 145, no. 12, p. dev165753, Jun. 2018, doi: <https://doi.org/10.1242/dev.165753>.
- [22] D. Kaltenecker, et al., Virtual reality-powered deep-learning analysis of brain cells, *Nat. Methods* 21 (7) (2024) 1306–1315, <https://doi.org/10.1038/s41592-024-02245-2>.
- [23] K.J. Friston (Ed.), *Statistical Parametric Mapping: The Analysis of Functional Brain Images*, 1st ed., Elsevier/Academic Press, Amsterdam ; Boston, 2007.
- [24] T.C. Pataky, One-dimensional statistical parametric mapping in Python, *Comput. Methods Biomed. Engin.* 15 (3) (2012) 295–301, <https://doi.org/10.1080/10255842.2010.527837>.
- [25] T.E. Nichols, A.P. Holmes, Nonparametric permutation tests for functional neuroimaging: a primer with examples, *Hum. Brain Mapp.* 15, no. 1, Art. no. 1 (2002), <https://doi.org/10.1002/hbm.1058>.
- [26] J. Piet, D. Hu, Q. Meslier, R. Baron, S.J. Shefelbine, Increased cellular presence after sciatic Neurectomy improves the bone Mechano-adaptive response in aged mice, *Calcif. Tissue Int.* 105 (3) (2019) 316–330, <https://doi.org/10.1007/s00223-019-00572-7>.
- [27] A.F. Pereira, B. Javaheri, A.A. Pitsillides, S.J. Shefelbine, Predicting cortical bone adaptation to axial loading in the mouse tibia, *J. R. Soc. Interface* 12 (110) (2015) 20150590, <https://doi.org/10.1098/rsif.2015.0590>.
- [28] K. Eller, et al., Mechanoadaptation of the bones of mice with high fat diet induced obesity in response to cyclical loading, *J. Biomech.* 124 (2021) 110569, <https://doi.org/10.1016/j.jbiomech.2021.110569>.
- [29] N. R. Gould et al., “Disparate bone anabolic cues activate bone formation by regulating the rapid lysosomal degradation of sclerostin protein,” *eLife*, vol. 10, p. e64393, Mar. 2021, doi:10.7554/eLife64393.
- [30] D. Sun, M.D. Brodt, H.M. Zannit, N. Holguin, M.J. Silva, Evaluation of loading parameters for murine axial tibial loading: stimulating cortical bone formation while reducing loading duration: EVALUATION OF LOADING PARAMETERS FOR MURINE AXIAL TIBIAL, *J. Orthop. Res.* (2017), <https://doi.org/10.1002/jor.23727>.
- [31] B. Javaheri et al., “Lasting organ-level bone mechanoadaptation is unrelated to local strain,” *Sci. Adv.*, vol. 6, no. 10, p. eaax8301, Mar. 2020, doi:<https://doi.org/10.1126/sciadv.aax8301>.